Int J Intell Robot Appl
DOI 10.1007/s41315-017-0022-x

REGULAR PAPER

Twisted and coiled polymer (TCP) muscles embedded in silicone elastomer for use in soft robot

Yara Almubarak[1] · **Yonas Tadesse**[1]

Received: 23 November 2016 / Accepted: 19 April 2017

Abstract Researchers are seeking to create robots that could conform to non-uniform objects during handling and manipulation. High performance artificial muscles are the key factors that determine the capabilities of a robot. Twisted and coiled polymeric (TCP) muscle embedded in soft silicone skin solves some of the problems of soft robots in attaining morphed structure using low voltages, contrary to other technologies such as dielectric elastomer and piezoelectric. Furthermore, the TCP actuation system does not generate noise like pneumatic systems. The TCP embedded skin shows great promise for robotics to mimic the flexible appendages of certain animals. In this paper, we present experimental results on the effect of muscle placement and the thickness of the artificial skin on the actuation behavior, which can be used as a benchmark for modeling. We demonstrate the effect of three different skin thicknesses and three different muscle locations within the skin, by taking experimental deformation data from stereo camera. In general, two modes of actuations (undulatory and bending) were observed depending on the muscle placement, skin thickness, applied voltage, and actuation time. The thinner skin showed two-wave undulatory actuation in most cases, whereas the 4 mm skins showed mixed actuation and the 5 mm skins exhibited one-wave undulatory actuation. In all cases, the increase in voltage resulted in higher magnitudes of actuation. In addition, we showed consistent strain of the TCP muscles from 18 samples from two batches that produced an average strain of 22% (batch 1) to 20% (batch 2) with standard deviation of 2.5–1.8% respectively.

Keywords Soft robots · TCP muscles · Artificial muscle · Biomimetic · Artificial skin

1 Introduction

Researchers have worked to come up with robots that are smooth in motion as a result of flexible structures. Numerous robotic skins were presented such as light soft silicone gel embedded with SMA (Tomar and Tadesse 2016), silicone embedded with Twisted and Coiled Polymer (TCP) muscles (Tadesse et al. 2016), silicone embedded with sensors such as force resistance sensor (Stiehl et al. 2004), temperature senor (Tomar and Tadesse 2016), and pressure sensor (Sanford et al. 2013). A compliant artificial muscle was also introduced, which can detect certain stresses using skin with microchannels filled with conductive liquids (Park et al. 2012). Another similar application is a hyperelastic pressure transducer that utilizes microchannels of conductive liquid eutectic gallium-indium (Park et al. 2010). Embedding sensors in a soft skin eliminates the use of extra space and sockets within the robot's structure, moreover, it gives it a smoother look. However, the motion performance of a robot is determined by the actuator used in the robot.

Electronic supplementary material The online version of this article (doi:10.1007/s41315-017-0022-x) contains supplementary material, which is available to authorized users.

✉ Yonas Tadesse
Yonas.Tadesse@utdallas.edu

Yara Almubarak
Yara.Almubarak@utdallas.edu

[1] Humanoid, Biorobotics and Smart Systems (HBS) Laboratory, Mechanical Engineering Department, Jonsson School, The University of Texas at Dallas, Richardson, TX 75080, USA

Published online: 26 April 2017

The development of soft robots requires advancement on soft actuating technology, control strategy, and locomotion method. Besides the traditional actuators like motors and pistons, many researchers have attempted to tackle the actuating technology by exploring different smart actuators. Smart actuators, such as shape memory alloys (SMAs), ionic polymer-metal composite (IPMCs), dielectric elastomer (DE), or piezoelectric have been proven to be a promising actuating solutions that can bring a good performance, a compact size, and a quiet operation; however they are expensive and consume higher voltages. Various biomimetic terrestrial robots have been presented by researchers (Majidi 2014). A caterpillar robot was introduced, which is capable of rolling through uneven surfaces and can adapt to different environmental conditions (Lin et al. 2011). Another terrestrial robot that operates using pneu-net, soft elastomeric chambers is also presented (Shepherd et al. 2011). A review of several new soft robots and the current challenges are summarized in Laschi et al. work(Laschi et al. 2016), covering terrestrial robot, underwater robots and other applications.

Regarding underwater robots, a micro-robot fish was developed based on an actuated biomimetic fin (Wang et al. 2008), which can bend easily due to an elastic substrate and embedded SMA wires. An undulating eel robot made of flexible polyurethane was introduced in (Low et al. 2006). In another related work, a robotic jellyfish called Robojelly was fabricated to mimic the structural features of the Aurelia aurita species using a bio-inspired shape memory alloy composite and RTV silicone (Villanueva et al. 2011). Moreover, a jellyfish model that is actuated by hydrogen and oxygen fuel was also proposed. The fuel-powered Robojelly uses nickel–titanium, multiwall carbon nanotube, nanoplatinum (NiTi/MWCNT/Pt) composite actuators that have been presented to mimic the natural movement of the jellyfish (Tadesse et al. 2012). Another biomimetic jellyfish robot was developed using IPMC actuators to implement jet propulsion (Yeom and Oh 2009). A lamprey-based undulatory vehicle (Wilbur et al. 2002), a free-swimming robotic batoid ray based on IPMC actuators (Chen et al. 2011), and a miniature fish-like robotic swimmer induced by propulsion generated by tail vibrations (Aureli et al. 2010) were presented. More recently, a swimming robotic fish was demonstrated that was developed with electromagnetic actuation system and 3D printing (Phamduy et al. 2017).

Creating robots that eliminate the use of heavy and bulky actuation units will broaden the new capabilities of a robot. New robotic skin was presented made of carbon black filled silicone for sensing surrounding environments (Lacasse et al. 2010). Inspired by previous literature, we propose a novel elastomeric skin embedded with actuators for ubiquitous use in the field of soft robotics. Recently, we presented similar embedded TCP muscles within silicone elastomer and various sensors for soft robot applications (Tomar and Tadesse 2016). However, the effect of the skin thickness and the placement of the muscles were not quantified. We also showed TCP muscles for icosahedron tensegrity robot (Wu et al. 2016), assistive devices, prosthetics or orthotic hands, and humanoid robotic hand (Wu et al 2015, 2017) and musculoskeletal system (Tadesse et al. 2016). The effect of skin thickness, placement of muscles and input power supplied to the muscles play the key role in the actuation behavior of the composite structure because all these parameters contribute to the static and dynamic behavior. In literature, there are some studies that show the relationships of shape changes due to configuration of the embedded muscles. One example is shape memory alloy embedded with laminated plate using finite element method (Park et al. 2004), and in-plane and out of plane actuation of SMA/elastomer composite (Feng et al. 2015). However, the authors showed few actuation of the composite. Another example is a micro aerial vehicle developed using macro fiber composite(MFC) (Bilgen et al. 2007; Ohanian et al. 2012). MFC is a piezoelectric composite material that was originally developed by NASA for morphing structures. MFC is made out of uniaxially aligned fibers embedded within a polymer matrix with interdigital electrode pattern, it is excellent flexible piezoelectric based actuators and can operate at high frequency. However, it is expensive (Tadesse et al. 2006).

In this paper, a novel artificial muscle embedded within silicone elastomer is discussed. The muscle is made by twisting and coiling a precursor fiber and applying heat treatment (Sahran and Tadesse 2016), we called this material, *Twisted and Coiled Polymer (TCP)* muscle throughout in this paper. Silicone elastomer material (Ecoflex-30) is used as an artificial skin material due to its elasticity and other imperative features. The EcoFlex-30 has a shore hardness of 00–30, up to 900% elongation at break, and a tensile strength of 200 psi(1379 kPa) (Smooth-on.com 2011). Silicone is also medically approved for breast implant and is translucent, which allows us to easily add color to achieve a more realistic model (Hedén et al. 2009). The TCP muscles are embedded within the skin to allow for full control of the skin and allow us to mold and attain the desired shape. By keeping the sensors embedded in the skin, safer human interaction with a robot can be achieved (Cannata et al. 2008). The muscles presented in this paper are used as linear actuators, which will result in artificial skin that can freely bend at different points to create the desired movements. Moreover, it is also cost effective and would be able to save more space compared to electrical and pneumatic actuators. There are no experimental results in the literature that show the actuation of the TCP muscles embedded in silicone. This is due to the recent introduction of the actuators

to the robotic community. Such experimental result could be a good asset for modeling and simulation for other researchers as well for our future use and a better understanding of the structure. If we refer to the structures found in nature, we see different architecture of morphed structures from elephant trunk, caterpillar wave motion, to fish motion. As seen in the right side of Fig. 1 such shapes could be achieved by changing the material and topology of our proposed structure to mimic those animal structures in the left side of Fig. 1. The paper is organized as follows: first, we will discuss the fabrication of the materials (skin and TCP muscles); second, experimental setup used for characterization will be presented; finally, experimental results and discussion will be proceeded.

1.1 Design and fabrication of the skin

The embedded skin proposed for soft robots is made of TCP muscles and low-shore hardness silicone elastomer that has equivalent stiffness to the soft tissue of animals. The fabrication process of the skin consists of three major steps: creating the skin molds, making the TCP muscles, and embedding the TCP muscle into the silicone material by casting a solution of room temperature vulcanized (RTV) silicone. The detail processes are explained in this section.

1.1.1 TCP muscle preparation

Twisted and Coiled Polymeric muscles were fabricated using automated fabrication system utilizing an DC motor using the same nylon precursor fiber from Shieldex Trading, Inc. and following our prior works (Wu et al. 2017; Saharan and Tadesse 2016). Essentially, the muscles were prepared from silver coated nylon 6,6 threads. TCPs are thermally driven actuators that can be triggered by applying voltage across terminal, similar to shape memory alloy. The fabrication process included the use of an electric motor on one end of the thread and a dead weight on the other end. The dead weight was placed at the end of the thread (precursor fiber) ensuring that each muscle was prepared using the same length thread. The twist was achieved by applying a counter clockwise rotation using

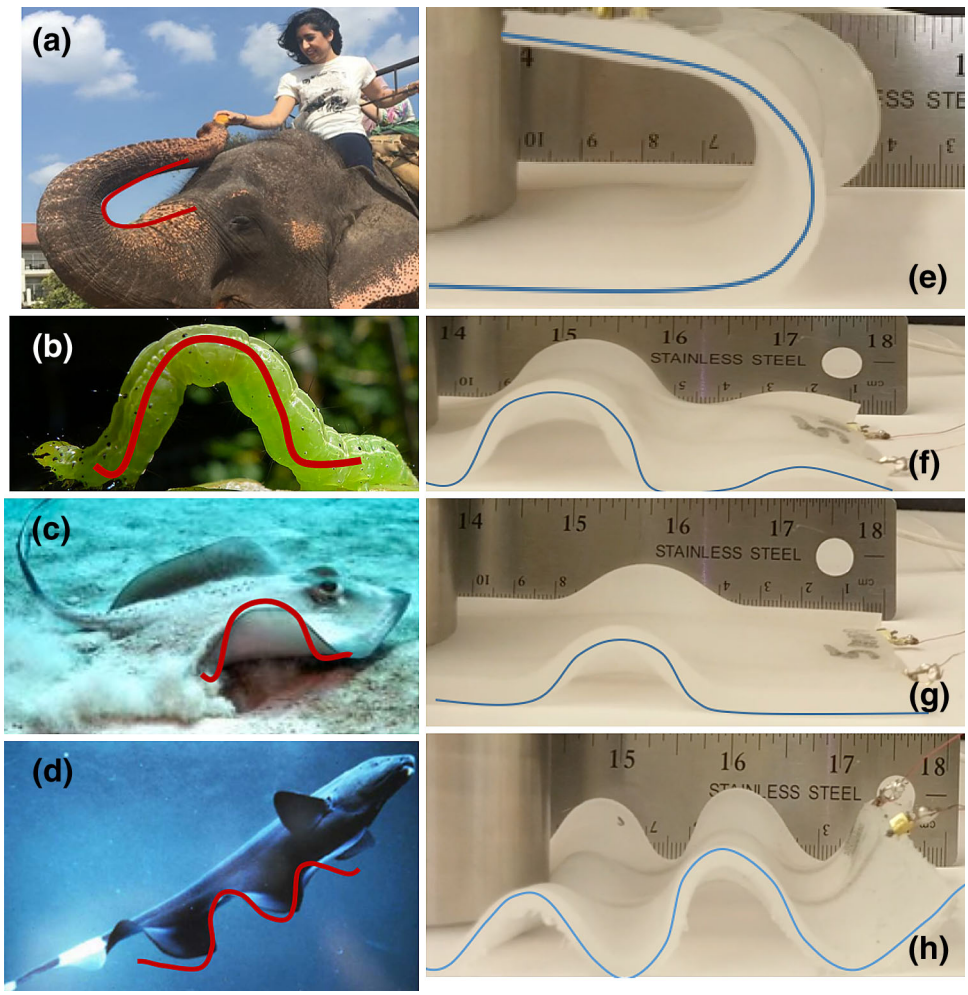

Fig. 1 Flexible structures found in nature: **a** Elephant trunk, courtesy of Yara Almubarak, **b** Caterpillar adulatory motion, courtesy of John Tann/Flickr, **c** Sting ray motion, courtesy of Gerard Soury/Oxford Scientific, **d** Electric ghost knife fish, courtesy of Roshi from recipeapart.com, and (**e**–**h**) TCP muscles embedded in silicone skin at different geometries and applied voltage

the motor. The twist caused the thread to coil, this coiling process is allowed to occur until the entire length of the thread is coiled, which is evaluated visually by observing the thread's change in diameter, this results in 1-ply muscle (Haines et al. 2014). In order to make 2-ply muscle, we folded the 1-ply in half, and due to the initial extreme twisting and coiling in the 1-ply, it coiled on itself. Each end is crimped to connect with power supply.

To study the effects of placement, 18 samples of 2-ply muscles (Fig. 2a) were fabricated, in batch 1 and 2. In batch 1, the muscles were then annealed by suspending 350 g dead weight and applying an increasing voltage proportional to the length of the TCP muscle using ($\sim$1.2 $\times$ length of the muscle in inches (Sahran and Tadesse 2016; Saharan and Tadesse 2016) until the muscle reaches steady state. The muscles were then trained by applying a voltage equal to the last annealing voltage, 7 V, and suspending a weight of 200 g (Fig. 2b). This voltage magnitude was applied to the muscles for 60 s period with 50% percent duty cycle (30 s ON and 30 s OFF). The annealing process was repeated 4 times for each annealing voltage, where the muscle reached its maximum length creating an annealed muscle. The training process was repeated 4 times for the final annealing voltage. In order to achieve the desired voltage at each process the current in the power supply was kept open while the voltage was set at a constant value. Data such as diameter, loaded and unloaded length, voltage, current, and strain are collected in the last cycle. Batch 2 was made in similar way except 8 V is used for annealing and training, also there was some difference in the initial unloaded length of each muscle. The results are provided in Table 1.

1.1.2 Skin molds

Three skin molds were created using computer aided design software (SolidWorks) and then 3-D printed using ABS material (Fig. 2c). Each mold is 140 mm long and 60 mm wide. The depths of each mold are 3, 4, and 5 mm respectively. Within the three molds are slots that are cut to center depth of each skin. These slots provide three different muscle locations within the skin and are placed at 10, 15, and 20 mm from the outer edge of the skin, which are referred as the outer, middle, inner muscle locations respectively throughout the remainder of this paper.

We observed that the cycle of training and the annealing cycle discussed before caused an average actuation of 22% (batch 1) and 20% (batch 2). The strain was calculated by using Eq. 1.

$$Strain(\%) = \frac{L_f - L_i}{L_i} 100 \quad (1)$$

Where L_f is the loaded length of the muscle and L_i is the initial length of the muscle before the applied voltage.

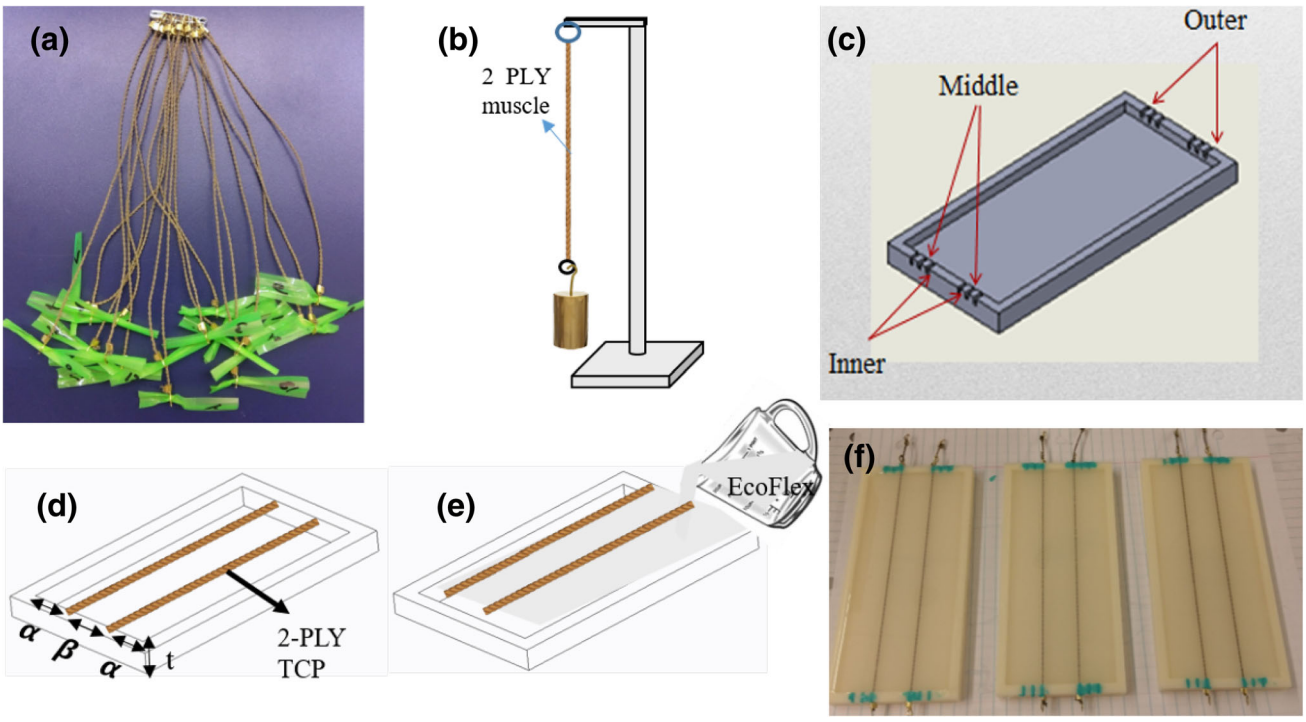

Fig. 2 Fabrication of the TCP muscles and the skin: **a** All 18 TCP samples, **b** Muscle training setup(350 g for annealing, 200 g for training), **c** CAD model of the mold showing different muscle locations, **d** and **e** Schematic diagram of embedding process, **f** Final result of skin curing in mold

Table 1 Parameters of the TCPs during Training at 200 g suspended weight, using 7 V (batch 1) and 8 V (batch 2) applied voltage

Muscle #	UL (mm)	LL (mm)	UD (mm)	LD (mm)	AD (mm)	SL (%)	I (A)	P (W)	P/LL (W/cm)
Batch 1									
1	169	185	1.20	1.03	45	24.32	0.70	4.90	0.26
2	190	210	1.10	0.89	45	21.43	0.66	4.62	0.22
3	190	205	1.10	0.92	45	21.95	0.65	4.55	0.22
4	175	181	1.20	1.00	46	25.41	0.70	4.90	0.27
5	185	200	1.26	1.10	50	25.00	0.74	5.18	0.26
6	165	180	1.19	1.05	40	22.22	0.65	4.55	0.25
7	180	190	1.30	1.13	40	21.05	0.69	4.83	0.25
8	170	180	1.12	0.95	40	22.22	0.76	5.32	0.30
9	174	185	1.19	1.02	40	21.62	0.74	5.18	0.28
Batch 2									
10	135	156	1.17	1.02	29	18.59	0.49	3.92	0.25
11	134	158	1.18	1.04	28	17.72	0.44	3.52	0.22
12	136	157	1.2	1.03	34	21.66	0.5	4	0.25
13	136	156	1.2	1.03	32	20.51	0.52	4.16	0.27
14	137	158	1.21	1.04	34	21.52	0.51	4.08	0.26
15	139	162	1.2	1.04	26	16.05	0.44	3.52	0.22
16	133	155	1.2	1.02	29	18.71	0.42	3.36	0.22
17	135	154	1.19	1.03	30	19.48	0.42	3.36	0.22
18	146	167	1.2	1.04	30	17.96	0.5	4	0.24

The length of the precursor fiber before twisting and coiling was 150 cm (batch 1) and 110 cm (batch 2)

UL unloaded length, *LL* loaded length, *UD* unloaded diameter, *LD* loaded diameter, *AD* actuation displacement, *SL* loaded strain, *I* current, *P* power, *P/LL* power/loaded length

1.1.3 Embedding process

In order to achieve equal actuation within both sides of the skin, muscle pairing was required. Using the data from Table 1, muscles with approximately the same loaded strain and current were paired together to be placed in the same mold. For example, muscle#4 and #5 have loaded strain equal to ~25% and current equal to ~0.7A; and muscle #12 and #14 had strain equal to ~21% while currents equal to ~0.5A. The muscles were then placed within the slots of the molds (Fig. 2d) kept tight with 200 g load and crimped, the extra length of muscles were cut. Once placed in the desired slot within the mold, the Ecoflex-30 material which consists of a 1:1 ratio mix of part A and B was poured (Fig. 2e) directly into the molds ensuring that the molds were full but not over flowing. All 9 molds were allowed to cure for at least 6 h at room temperature of 21.1 °C. Three samples of the skin with equal spacing but different thickness are shown in Fig. 2f.

2 Experimental set up

After fabricating the skin embedded with TCP muscles, tests were conducted to measure their performances. The experimental set up included the skin samples with embedded muscles, power supply, wires for electrical connection, Stereo camera (ZED^{TM} 2 k stereo camera from Stereolabs company) to capture the skin deformation. Copper wires were used to connect the TCP muscles to the voltage source, the skin was mounted on a flat surface, one end is securely fixed by applying a 500 g weight, and the other end was set free to move. Black points were added on the edge of the skin to accurately quantify the data and obtain the skin deformation along the X, Y axis. While red points were used on a frame as a reference to be used in converting pixel values to mm. The experimental set up is shown in the schematic diagram, Fig. 3a and the actual picture is shown in Fig. 3b.

2.1 Procedures for testing the skin

The following steps were followed to measure the deformation of the skin when voltages of 9, 10, and 11 V were applied to the TCP muscles. Lower magnitude of voltage did not provide significant actuation and therefore are not presented. The purpose of this experiment was to measure the type of deformations that are resulted according to the different thicknesses of the fabricated skin. Three different skin thickness, 3, 4, and 5 mm were tested. DC voltages were applied for 40 s for all the

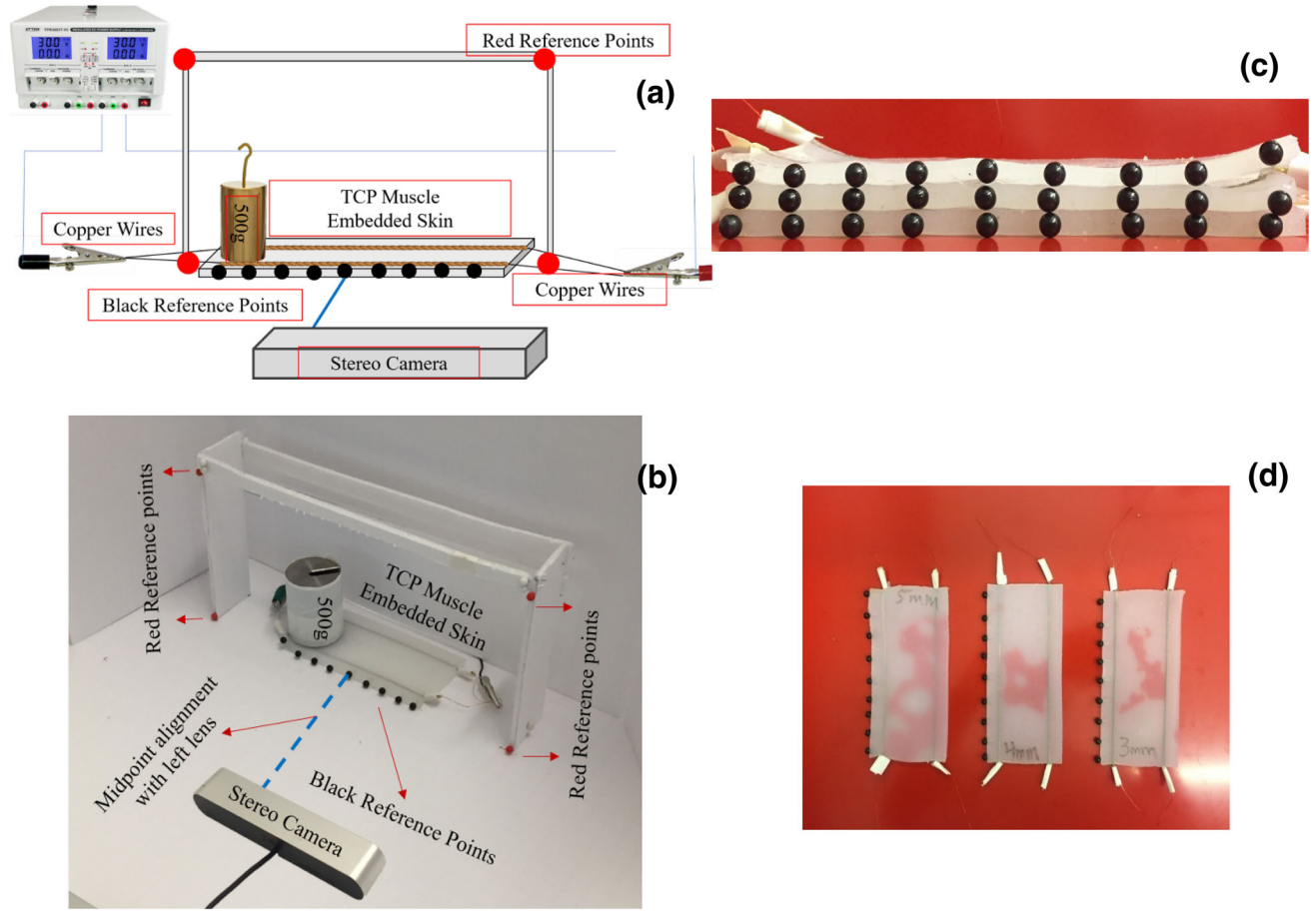

Fig. 3 Experimental setup for testing the skin: **a** Schematic diagram, **b** Photograph of the actual test set up, **c** Side view of all skins with $\beta = 40$ mm and *black points* aligned, and **d** Top view of skin samples with *black points*

samples. After applying voltages, the skin was allowed to cool down for 5 min before it was used again for higher voltages to allow us to quantify each data set individually without the influence of previous experiments. This process was repeated for all 9, 10, and 11 V. TCPs are low speed actuators when stimulated by square wave, similar to SMAs and this is due to the longer time they require to heat and cool the structures. Even when embedded within the skin, they require more time for heat dissipation. Therefore, sufficient time gap between experiments is necessary for such actuators.

2.2 Determining the skin deformation using camera

A stereo camera was used to measure skin motion following the flow chart shown in Fig. 4. Nine black points were added to skin separated equally to allow the camera to capture the skin's deformation throughout the whole skin. In addition, four red markers were used for a reference frame. The frame plane and the skin's edge were parallel on the same axis. The camera was orthogonal to the skin edge and the center of the left camera lens was aligned with the center point of skin's edge, Fig. 4c. The camera model is "ZED" from SteroLabs. Generally, stereo cameras are modeled by two pinhole cameras (Gremban et al. 1988). A checkerboard was used to extract the camera's parameters and lenses distortions (Heikkila and Silven 1997; Tomasi and Kanade 1992; Zhang 2000). The camera took a stereo image in every 10 s period for a total time of 40 s. Then, the stereo images are rectified by the camera parameters. By trial and error, we did some basic operation (addition, subtraction, etc.) on color channels (red, green, and blue) of the left camera image to gain a proper single channel for each red and black marker. Then, binary images are extracted by thresholding. The binary images have some unwanted noise; these noises were canceled by using morphologically close image function. The result is two noise free binary images, one for the black markers and one for the red markers. Then, coordinates of center of each markers were calculated in pixel and stored. At the end, the planar motion of black markers (skin) are computed in millimeter unit by assumption of orthographic projections (Zhang 2000). The skin deformation is then processed in MATLAB.

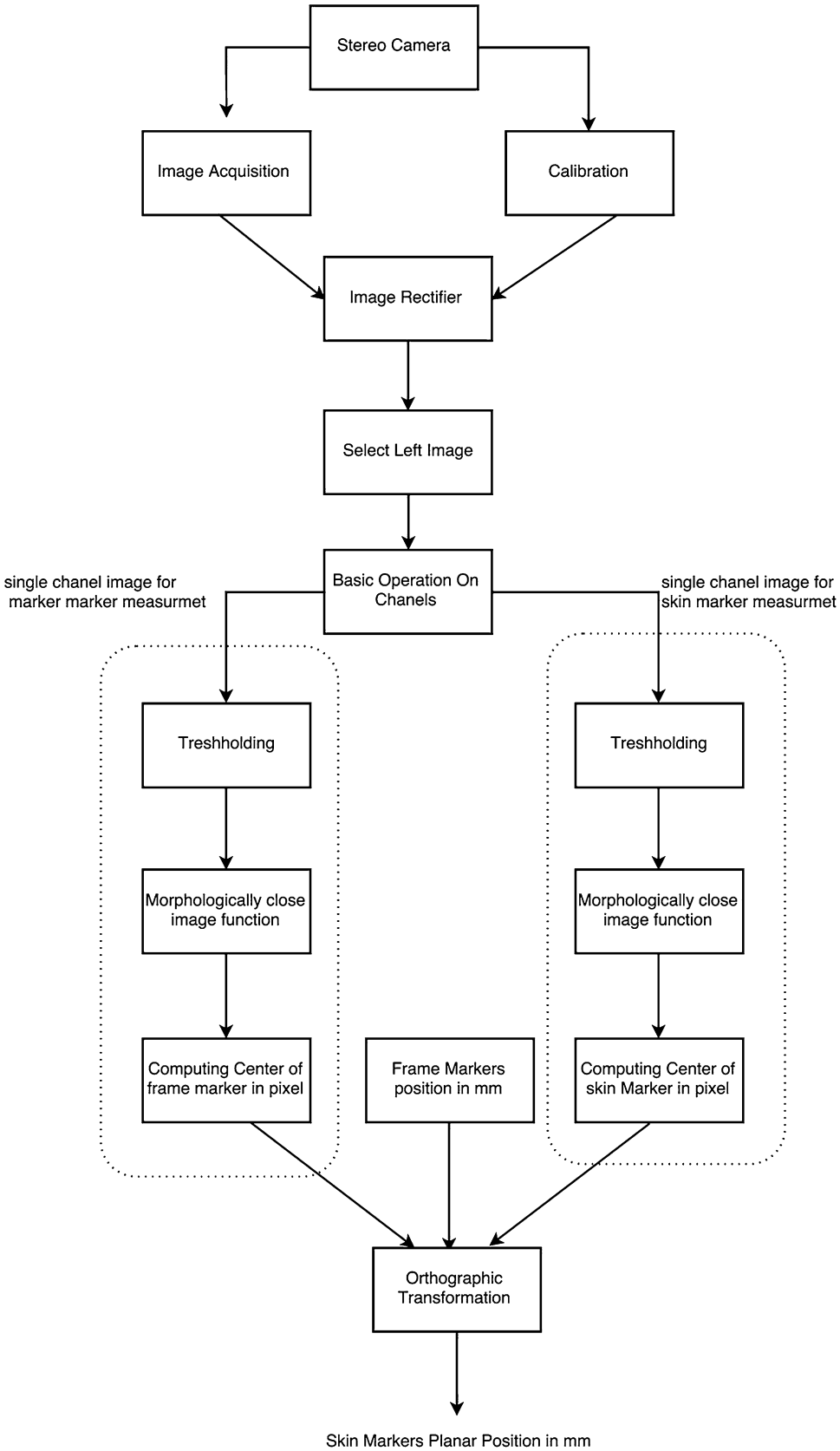

Fig. 4 Flow chart of camera processing to determine skin deformation

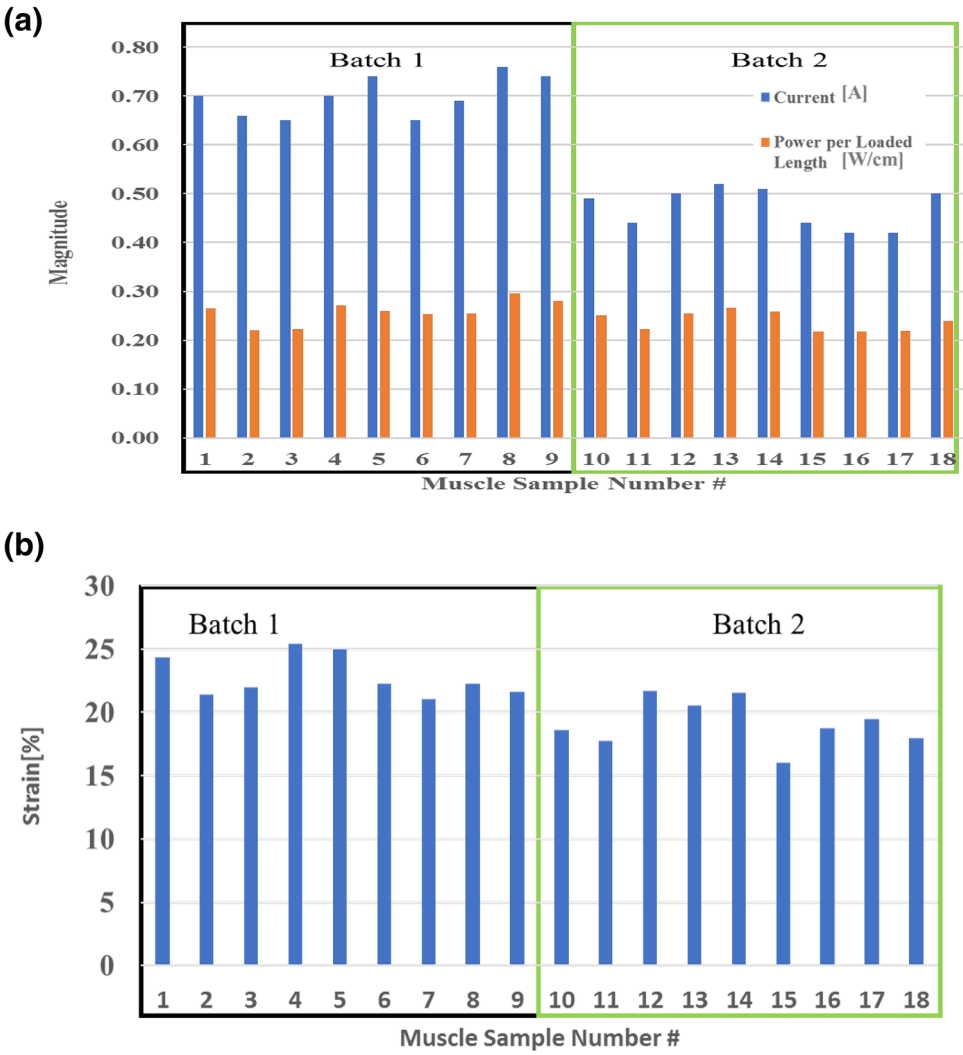

Fig. 5 Experimental results of TCP muscles: **a** Electrical current [A] and Power/Length [W/cm] given to the TCP muscle samples, and **b** Strain of each TCP muscle samples, 16–25%

3 Results and discussion

3.1 Effect of variation of muscles

One of the concerns of the newly introduced TCP muscles is the reliability or the consistency of the actuation performance. To study the variation of strain, as discussed at the beginning of this paper, we made 18 muscle samples of lengths 175 mm ± 9.2 mm (batch 1) and 136 mm ± 3.8 mm (batch 2) with the same processing conditions. The muscles were tested under the same conditions and the DC current consumption of each muscles was 0.59 A with standard deviation of 0.12A. The power per loaded length of the muscle was on average 0.25 W/cm with a

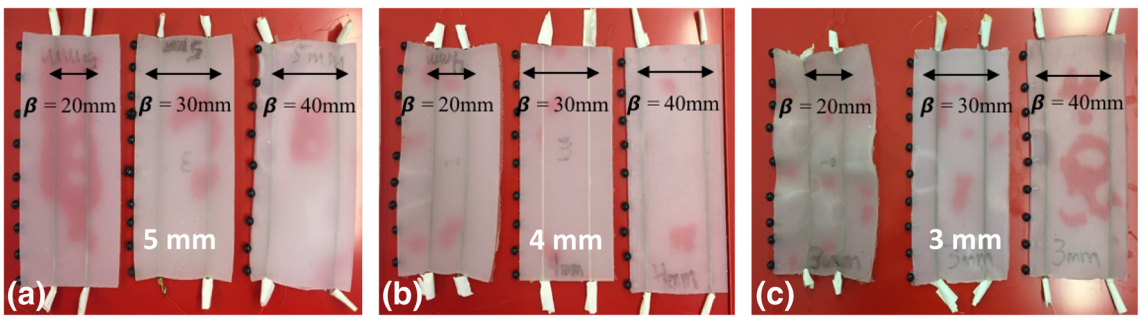

Fig. 6 Samples of all TCP embedded in skin: **a** 5 mm thick skin, **b** 4 mm thick skin, and **c** 3 mm thick skin

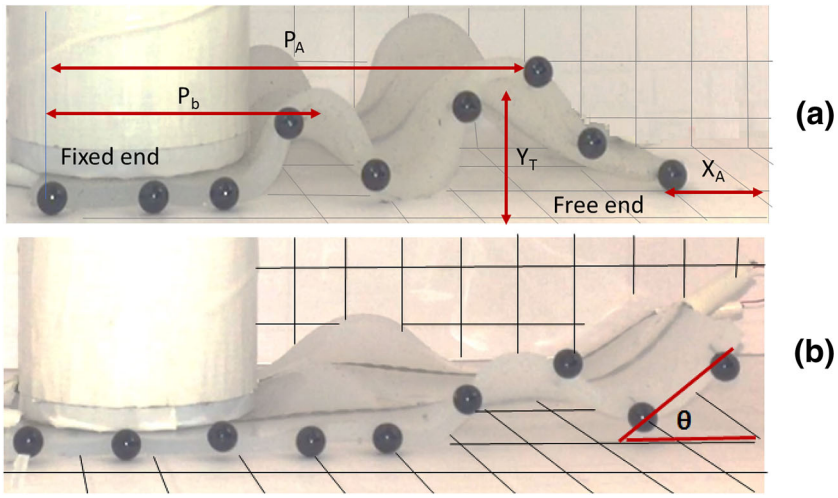

Fig. 7 Typical actuation mode of embedded TCP muscles showing axial and transversal motions: **a** mode I -deformation along X axis, X_A; deformation along Y axis, Y_T; closest peak distance from fixed point, P_b; farthest peak distance from fixed point, P_A. **b** Mode II-angle formed with the edge of the free end, θ

Table 2 Muscle pairing parameters according to data from Table 1

Skin thickness/muscle location	Muscle number #	Strain (%)	Current (A)
3 mm inner	1,6	24–22	0.70–0.65
3 mm middle	4,5	25–25	0.70–0.74
3 mm outer	17,18	19–18	0.42–0.5
4 mm inner	2,3	21–22	0.66–0.65
4 mm middle	10,16	19–19	0.49–0.42
4 mm outer	9,13	22–21	0.74–0.52
5 mm inner	11,15	18–16	0.44–0.44
5 mm middle	12,14	22–22	0.50–0.51
5 mm outer	7,8	21–22	0.69–0.76

standard deviation of 0.02 W/cm, Fig. 5a. All the electrical power are provided from direct current (DC) source, not AC source. The actuation strain was on average 22% (batch 1) to 20% (batch 2) with standard deviation of 2.5–1.8% respectively, Fig. 5b. The current (max 0.7A), power per length (max 0.3 W/cm) and strain (max 25%) results for the muscles are shown in Fig. 5. It should be noted that higher current magnitude of 0.3–0.5A are considered to be dangerous at higher voltage. However the voltage magnitude and the frequency in which the skins are tested are low (max 11 V). Therefore, the electrical power applied will not be a major concern. In addition, the silicone skin as a dielectric material with high impedance prevent damage due to electrical shocks. The actuation magnitude shown in Fig. 5b demonstrates that the 18 muscles showed reliable strain to use them in many robotic systems. Therefore, the consistency and repeatability of the TCP muscles is very good when using the same precursor fiber and training method, when two different batched are prepared from different precursor fiber, some variations were observed. This could be due to the silver coating difference and slight manufacturing process steps. One of the drawbacks of TCPs is the efficiency which is low (1–2%) similar to shape memory alloy (SMA) actuators.

3.2 Effects of TCP muscle placement and skin thickness

Before conducting the main experiment, there are several results that can be concluded about muscle placement and skin thickness. The TCP muscles were in tension during the molding by stretching them in the mold and crimping. When the skins were released from the mold, the tension in the muscles were transferred into the silicone skin. The resulting tension had varying effects on the skin based on the muscle placement and silicone thickness. The muscle placement within the 5 mm thick skin showed no visible effect. The muscle placement on the 3 mm thick skin showed bulges on the inner positions ($\beta = 20$ mm), while the middle and outer position showed no deformation ($\beta = 30$ mm, $\beta = 40$ mm) respectively. Figure 6 shows the structures of the skin fabricated for parametric study, from left to right, the skin thickness 5 mm to 3 mm with different spacing (β) along with the bulges at the edges are shown.

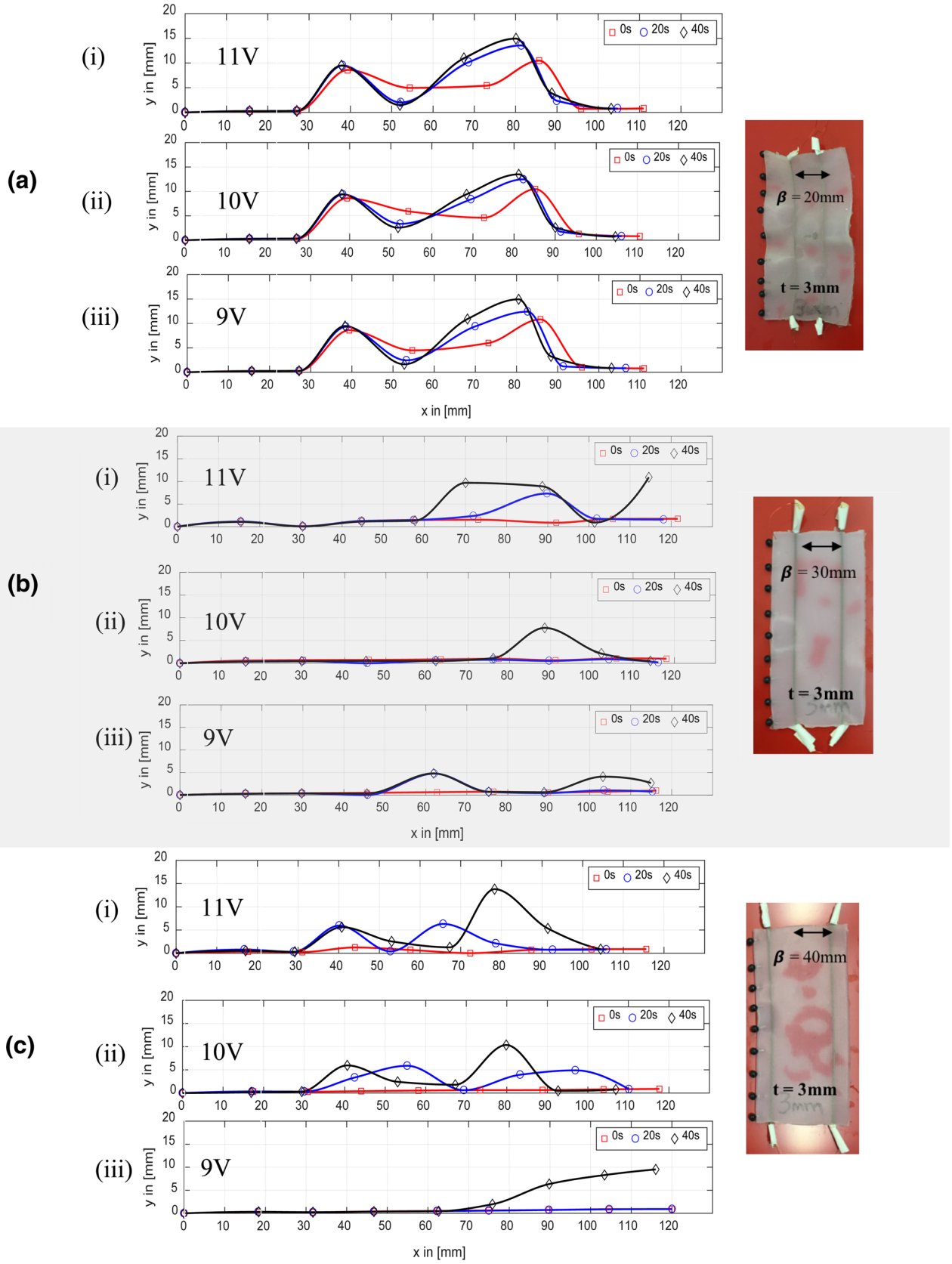

Fig. 8 Deformation of 3 mm thick skin for various input voltages, at different times and muscle positions: **a** β = 20 mm, **b** β = 30 mm, and **c** β = 40 mm. [i] at 11 V, [ii] at 10 V, [iii] at 9 V

Table 3 Actuation characteristics of 3 mm skin with different placement of muscles

Muscle position	Voltage (V)	X_A (mm)	Y_T (mm)	P_A (mm)	P_b (mm)	θ (deg)
Inner, β = 20 mm	9	9	14	80	37	0
	10	8	15	82	36	0
	11	7	14	83	38	0
Middle β = 30 mm	9	2	5	105	62	11
	10	5	7	0	90	0
	11	7	10	0	80	39
Outer β = 40 mm	9	5	10	0	0	12
	10	10	11	80	40	0
	11	12	14	77	40	0

3.3 Actuation test of the TCP embedded skin

All the skin samples discussed in the previous section were tested for performance. It was noted that all the skins did not actuate until a minimum of 8 V was applied. As the voltages increased to a maximum of 11 V, the actuations within the skins also increased and showed various morphed shapes. The specific shapes are dependent on the skin thickness and placement of muscles. Typical actuation of the skin can be described by Fig. 7 in two different modes (Mode I and Mode II), there are axial motion (X_A) parallel to the muscles, there are transversal displacement and formation of bulges (Y_T, maximum vertical deformation), the period length between bulges (P_A and P_B), and (θ) angle formed with the edge at the free end.

3.3.1 Muscle pairing

As discussed earlier, the muscle pairing was done based on the equal performance during actuation. Table 2 shows detailed information for muscle pairing for all skin thickness and muscle pairings.

3.3.2 Actuation behavior of 3 mm thick skin

First, the 3 mm thick skin with the inner muscle (β = 20 mm) had already bulged structures due to the prestress. At the beginning of actuation at 9 V (comparing t = 0 s and t = 40 s), the muscle deformed along the x-axis and y axis as shown in Fig. 8a (iii). At the higher voltage 10 V, presented in Fig. 8a (ii), similar deformation was observed but with increasing magnitude. The top row of Fig. 8a shows that at 11 V the waveform of the skin became slightly higher at t = 40 s compared to the 10 V at 40 s. No significant change for P_A and P_b was observed. Second, the skin with middle muscle location at (β = 30 mm), at the 9 V and 10 V, the free end changed along the x axis slightly while the bulges increased in height which can be observed in Fig. 8b (ii, iii). At the higher voltage, 11 V, Fig. 8b (i) shows the free end had changed significantly along the x axis and y axis similar to the previous voltages, as well as the free end lifted up with an angle of 39^0 at t = 40 s. The 9 V showed two peaks (P_A and P_b), while the 10 V and 11 V only observed one peak (P_A). Third, the skin with the outer muscle (β = 40 mm) was analyzed. The 9 V actuation resulted the free end t to lift up with angle 12^0 shown in Fig. 8c (iii). The change in X_A was not significant. Both the 10 V and 11 V actuation resulted in an increase along the x axis and y axis. Moreover, it is observed that they both developed two peaks throughout the whole structure of the skin as seen in Fig. 8c (i, ii). Table 3 shows the deformation data for the 3 mm thick skin for all muscle locations with respect to the characteristic curves shown in Fig. 7. All comparisons were taken when the time was changed from 0 to 40 s (black and red lines in the plots).

3.3.3 Actuation behavior of 4 mm thick skin

The 4 mm thick skin with inner muscle (β = 20 mm) did not exhibit bulges like the 3 mm thick skin. At all three voltages (9 V, 10 V, and 11 V), similar actuations were observed. The free end lifted up with a maximum angle θ of 60^0 and there was a slight change in X_A as shown in Fig. 9a (i–iii). On the other hand, the skin with middle muscle (β = 30 mm) acted differently. At 9 V very little actuation was observed, the fixed end was lifted up (bending motion) of the skin as seen in Fig. 9b (iii). At 10 V and 11 V Fig. 9b (i, ii), the skin deformed linearly (X_A) and two bulges were created in the skin with increasing magnitude as the voltage increased at 40 s actuation time. Furthermore, the skin with outer muscle (β = 40 mm) showed significant deformation throughout all voltages. At 9 V the free end lifted and deformed linearly along the x axis Fig. 9c (iii). While at 10 and 11 V, the free end lifted up significantly compared to 9 V, with a difference of ∼10 mm. Two bulges were also created throughout the skin. All deformation data are demonstrated in Table 4.

3.3.4 Actuation behavior of the 5 mm thick skin

The 5 mm thick skin with inner muscle (β = 20 mm), for both 9 V and 10 V no actuation was observed as demonstrated in Fig. 10a (ii, iii). On the other hand, at 11 V the skin formed significant deformation as it moved about both x and y axis. The free end also lifted at a maximum angle of θ ∼ 15 degrees measured from the midpoint of P_A bulge. While the skin with middle muscle (β = 30 mm) had actuation similar to inner muscle at 11 V but larger in magnitude as shown in Fig. 10b (i–iii). Significant

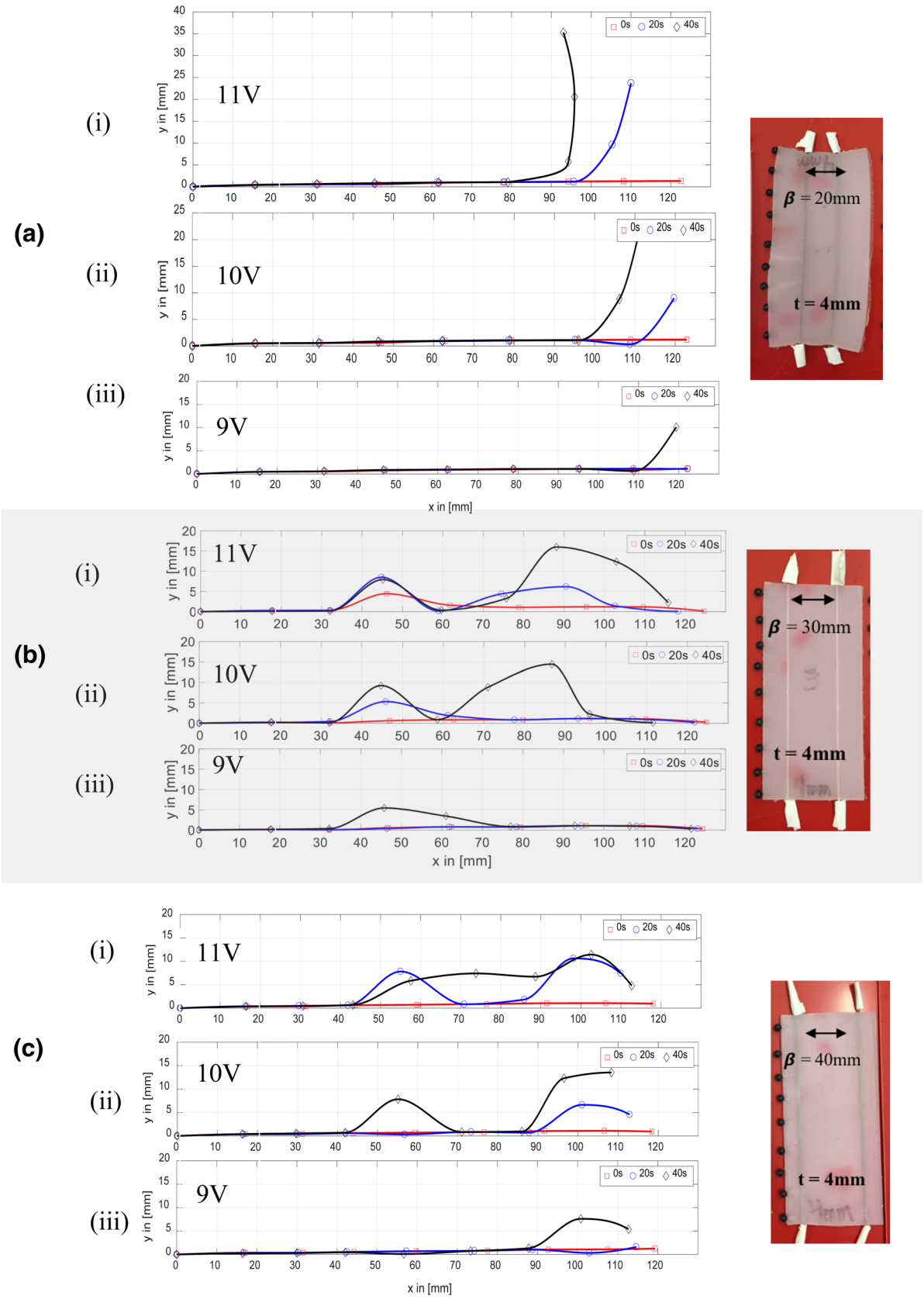

Fig. 9 Deformation of 4 mm thick skin for various input voltages, at different times and muscle positions: **a** β = 20 mm, **b** β = 30 mm, and **c** β = 40 mm. [i] at 11 V, [ii] at 10 V, [iii] at 9 V

Table 4 Actuation characteristics of 4 mm skin with different placement of muscles

Muscle position	Voltage (V)	X_A (mm)	Y_T (mm)	P_A (mm)	P_b (mm)	θ (deg)
Inner, β = 20 mm	9	4	10	0	0	45
	10	10	25	0	0	66
	11	30	35	0	0	27
Middle β = 30 mm	9	3	5	0	45	0
	10	14	15	88	45	0
	11	10	16	88	44	3
Outer β = 40 mm	9	7	7	0	100	9
	10	11	13	95	55	26
	11	5	11	102	55	7

difference in all parameters of X_A, Y_T, and peaks (P_A, P_b) were observed while still maintaining the same shape of deformation throughout all voltages. Additionally, the skin with outer muscle (β = 40 mm) did not show much change. Small bulges were formed throughout the edge of the skin and little movement within the x axis was observed, seen in Fig. 10c. Observing from Fig. 10c (ii), Y_T is moved slightly downwards due to the tension on the muscles where the skin formed bulges as the time increased. Table 5 summarizes all the data for the 5 mm thick skin.

Supplementary information about the skin characteristics are given in appendix. Appendix A1–A3 show the 3D plots (deformation along x-axis, y axis and time axis) as well as the snapshot of the skin at different voltage and time.

3.4 Discussion on the actuation behavior of the skins

By observing the actuation results for different muscle placement and skin thickness, different soft morphed structures were obtained. These soft structures are dependent on the input voltage to the muscles (indirectly the heat provided to the muscles), the time the voltage is applied, the thickness of the skin, the placement of the muscles, the elasticity of the skin and the boundary condition of the skin. The embedded muscles required high voltage to actuate. This is because the heat of the muscle is taken by the elastomer skin due to conduction when powered electrically, in embedded condition. Therefore, higher voltage is required to raise the temperature via resistive heating. The higher the voltage the more actuation/deformation was observed for all the skin samples (Figs. 8, 9, 10), this is obvious and to be expected. Considering the muscle placement in a skin sample, the increase of β caused different actuation results for all skin samples.

- For 3 mm thick skin at constant voltage 9 V, at β = 20, large bulges (15 mm in amplitude) were observed; at β = 30 smaller bulges (5 mm in amplitude) at the middle were obtained; and at β = 40 no bulges were formed, instead the free end lifted up 12^0 (mode II actuation). This can be seen in Fig. 8a–c, all iii. One of the reasons is that the smaller spacing resulted in local deformation, the muscles are closer to each other and higher axial force is applied at central region of the skin, and caused bulge formations (mode I actuation). For this 3 mm skin, at higher voltage (11 V), the effect of β created mixed mode actuation (mode I and mode II, Fig. 8a–c, all i). The switching happened at β = 30 mm.
- For 4 mm thick skin, at the same voltage (9 V), the increase in β resulted a mixed mode of actuation, at β = 20, mode II, β = 30, mode I and β = 40, mode II were observed, Fig. 9a–c, all iii. At higher voltage (11 V), mode I and II actuations were observed, Fig. 9a–c, all i. The reason for such variation is the combination of thickness, muscle placement, applied voltage and actuation time. It can be seen that at 11 V, at β = 20 mm, the muscles are closer to each other and the skin lifted up like a rigid cantilever.
- The same explanation applies to the 5 mm thick skin. The 5 mm thick skin had only one bulge along the length. This is due to the thickness of the skin that prevents the formation of bulges, due to its higher bending stiffness. Bending like a rigid cantilever beam was not observed in this skin like the 4 mm skin, even if the free end bends, it always results in a downward bent curve due to the hanging weight as seen in Fig. 10a, b. Most of the behaviors of the skins (for all samples) cannot be easily expressed.
- Recently, we presented a study on 2-ply TCP muscles prepared in similar manner but slightly different parameters and showed that an effective force of ~2.5 N for an applied power of 0.28 W/cm (Wu et al. 2017) can be obtained. If the power changes from 0.21 to 0.17 W/cm, the force reduces from 2 to 1.8 N. Therefore, for the current study, not only the force but the other parameters of the skin, thickness, spacing between muscles, elasticity of the skin and duration of actuation play the key role. It is difficult to explicitly state when the mode of actuation occur as it is the combination of the variables described above.

We conclude that this type of technology is very versatile. The soft robotic skin can be used in applications related to biomimetic robots both terrestrial and underwater robots. The TCP soft skin actuation is similar to many animal movements such as the caterpillar, water creatures, or even the elephant's trunk as discussed previously in

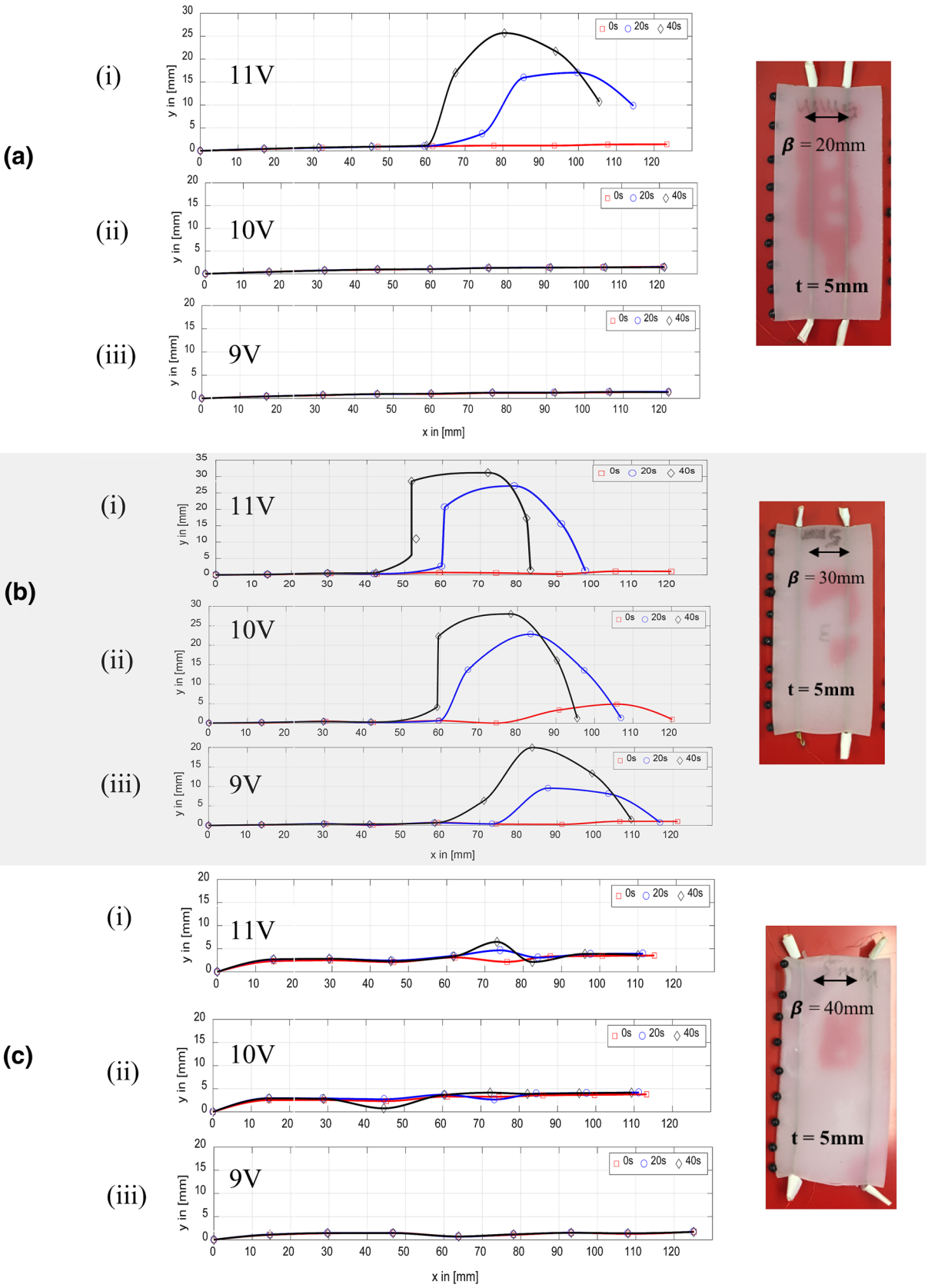

Fig. 10 Deformation of 5 mm thick skin for various input voltages, at different times and muscle positions: **a** β = 20 mm, **b** β = 30 mm, and **c** β = 40 mm. [i] at 11 V, [ii] at 10 V, [iii] at 9 V

Table 5 Actuation characteristics of 5 mm skin with different placement of muscles

Muscle position	Voltage (V)	X_A (mm)	Y_T (mm)	P_A (mm)	P_b (mm)	θ (deg)
Inner, β = 20 mm	9	0	0	0	0	0
	10	0	0	0	0	0
	11	17	25	0	80	15
Middle β = 30 mm	9	12	20	0	83	4
	10	25	28	0	80	4
	11	21	30	0	70	3
Outer β = 40 mm	9	0	0	0	0	0
	10	3	−3	43	75	0
	11	5	7	0	72	0

Fig. 1. We would be able to create robots that are similar to these animals without the use of servo motors, making this lighter in weight which gives them a more fluidic motion. TCPs are extremely useful due to their high actuation, simple fabrication methods and low cost. Some of the drawbacks of this actuators is the low efficiency and slow speed. This low efficiency and speed are the same for other smart materials such as shape memory alloy (SMAs). There are some solutions to improve the speed of the actuators such as using active cooling (Tadesse et al. 2010; Yip and Niemeyer 2015), or pulsed actuation (Wu et al. 2017). To improve the low efficiency, locking mechanism can be employed to conserve the energy usage(Saharan and Tadesse 2016).

4 Conclusion

In this paper, we showed experimental results on the actuation behavior of embedded 2-ply TCP muscles within the skin of 140 × 60 mm length and width. We quantified the effect of skin thickness and muscle placement. Results showed that both factors (thickness and placement) play significant role in not only on the actuation behavior of the skin but also the skin's overall appearance. In general, two modes of actuations (undulatory and bending) were observed depending on the muscle placement, thickness of the skin, applied voltage, and actuation time. The thinner skins (3 mm) showed two-wave undulatory actuation in most cases, whereas the 4 mm skins showed mixed actuation (both undulatory and bending) and the 5 mm skins exhibited one-wave undulatory actuation (Figs. 8, 9, 10). In all cases, the increase in voltage resulted in higher magnitudes of actuation. The bulges produced by some of the skins are perfect for biomimetic soft robotics. To determine the reliability of the TCP actuators, 18 samples were fabricated and tested providing consistently an average strain of 22% for batch 1 and 20% for batch 2. Three different thicknesses (3, 4 and 5 mm) of skin were developed, each consisting of three different spacing (20, 30 and 40 mm gaps between two muscles) for muscle positioning that allowed us to study nine different muscle scenarios. These structures showed different morphing behaviors depending on the applied voltage and muscle configuration that can mimic the flexible structure of natural organisms such as a caterpillar, an elephant trunk, under water creatures such as ghost knife fish, and others. This conclusion is based on skins made from Eco-Flex 30 which is more rigid than other available silicones. Further testing should be done using other type of silicone elastomer to determine an optimized artificial muscle-skin structure. We hope that the results presented in this paper will be relevant to other researches who would like to model the structure or create different types of biomimetic robots.

Acknowledgements We would like to acknowledge the support of ONR under Grant N00014-15-1-2503. We also would like to thank Andrew Toliver for his help during the initial work of this study.

References

Aureli, M., Kopman, V., Porfiri, M.: Free-locomotion of underwater vehicles actuated by ionic polymer metal composites. IEEE/ASME Trans. Mechatron. **15**(4), 603–614 (2010)

Bilgen, O., Kochersberger, K., Diggs, E., Kurdila, A., Inman, D.: Morphing wing micro-air-vehicles via macro-fiber-composite actuators. In: 48th AIAA/ASME/ASCE/AHS/ASC Structures, Structural Dynamics, and Materials Conference. p. 1785 (2007)

Cannata, G., Maggiali, M., Metta, G., Sandini, G.: An embedded artificial skin for humanoid robots. In: Multisensor Fusion and Integration for Intelligent Systems, 2008. MFI 2008. IEEE International Conference on pp. 434–438. IEEE (2008)

Chen, Z., Um, T.I., Bart-Smith, H.: A novel fabrication of ionic polymer–metal composite membrane actuator capable of 3-dimensional kinematic motions. Sens. Actuators A **168**(1), 131–139 (2011)

Feng, N., Liu, L., Liu, Y., Leng, J.: Characteristics of multi-functional composites using elastomer embedded with Shape Memory Alloy wires. Mater. Des. **88**, 75–81 (2015)

Gremban, K.D., Thorpe, C.E., Kanade, T.: Geometric camera calibration using systems of linear equations. In: Robotics and

Automation, 1988. Proceedings., 1988 IEEE International Conference on. pp. 562–567. IEEE (1988)
Haines, C.S., et al.: Artificial muscles from fishing line and sewing thread. Science **343**(6173), 868–872 (2014)
Hedén, P., et al.: Long-term safety and effectiveness of style 410 highly cohesive silicone breast implants. Aesthetic Plast. Surg. **33**(3), 430–436 (2009)
Heikkila, J., Silven, O.: A four-step camera calibration procedure with implicit image correction. In Computer Vision and Pattern Recognition, 1997. Proceedings., 1997 IEEE Computer Society Conference on. pp. 1106–1112. IEEE (1997)
Lacasse, M.-A., Duchaine, V., Gosselin, C.: Characterization of the electrical resistance of carbon-black-filled silicone: Application to a flexible and stretchable robot skin. In: Robotics and Automation (ICRA), 2010 IEEE International Conference on. pp. 4842–4848. IEEE (2010)
Laschi, C., Mazzolai, B., Cianchetti, M.: Soft robotics: Technologies and systems pushing the boundaries of robot abilities. Sci. Robot., vol. 1, no. 1, p. eaah3690 (2016)
Lin, H.-T., Leisk, G.G., Trimmer, B.: GoQBot: a caterpillar-inspired soft-bodied rolling robot. Bioinspir. Biomim. **6**(2), 026007 (2011). doi:10.1088/1748-3182/6/2/026007
Low, K.H., Yang, J., Pattathil, A.P., Zhang, Y.: Initial prototype design and investigation of an undulating body by SMA, In: 2006 IEEE International Conference on Automation Science and Engineering. pp. 472–477. IEEE (2006)
Majidi, C.: Soft robotics: a perspective—current trends and prospects for the future. Soft Robotics **1**(1), 5–11 (2014)
Ohanian, O. et al.,: Piezoelectric morphing versus servo-actuated MAV control surfaces. In: 53rd AIAA/ASME/ASCE/AHS/ASC Structures, Structural Dynamics and Materials Conference 20th AIAA/ASME/AHS Adaptive Structures Conference 14th AIAA, p. 1512 (2012)
Park, Y.-L., Chen, B.-R., Wood, R.J.: Design and fabrication of soft artificial skin using embedded microchannels and liquid conductors. IEEE Sens. J. **12**(8), 2711–2718 (2012)
Park, J.-S., Kim, J.-H., Moon, S.-H.: Vibration of thermally post-buckled composite plates embedded with shape memory alloy fibers. Compos. Struct. **63**(2), 179–188 (2004)
Park, Y.-L., Majidi, C., Kramer, R., Bérard, P., Wood, R.J.: Hyperelastic pressure sensing with a liquid-embedded elastomer. J. Micromech. Microeng. **20**(12), 125029 (2010)
Phamduy, P., Vazquez, M.A., Kim, C., Mwaffo, V., Rizzo, A., Porfiri, M.: Design and characterization of a miniature free-swimming robotic fish based on multi-material 3D printing. Int. J. Intell. Robot. Appl. (2017). doi:10.1007/s41315-017-0012-z
Saharan, L., Tadesse, Y.: Robotic hand with locking mechanism using TCP muscles for applications in prosthetic hand and humanoids. In: SPIE Smart Structures and Materials + Nondestructive Evaluation and Health Monitoring, pp. 97970 V–97970 V–9: International Society for Optics and Photonics (2016)
Sahran, L., Tadesse, Y.: Fabrication parameters and performance relationship of twisted and coiled polymer muscle. IMECE (2016)
Sanford, J., Ranatunga, I., Popa, D.: Physical human-robot interaction with a mobile manipulator through pressure sensitive robot skin, in: Proceedings of the 6th International Conference on PErvasive Technologies Related to Assistive Environments, p. 60. ACM (2013)
Shepherd, R.F., et al.: Multigait soft robot. Proc. Natl. Acad. Sci. **108**(51), 20400–20403 (2011)
Smooth-on.com: Ecoflex® Series Super-Soft, Addition Cure Silicone Rubbers. (ed.) p. 2 (2011)
Stiehl, W.D., Lalla, L., Breazeal, C.: A somatic alphabet approach to sensitive skin, in Robotics and Automation. Proceedings. ICRA'04. 2004 IEEE International Conference on, 2004, vol. 3, pp. 2865–2870. IEEE (2004)
Tadesse, Y., Priya, S., Stephanou, H., Popa, D., Hanson, D.: Piezoelectric actuation and sensing for facial robotics. Ferroelectrics **345**(1), 13–25 (2006)
Tadesse, Y., Thayer, N., Priya, S.: Tailoring the response time of shape memory alloy wires through active cooling and pre-stress. J. Intell. Mater. Syst. Struct. **21**(1), 19–40 (2010)
Tadesse, Y., Villanueva, A., Haines, C., Novitski, D., Baughman, R., Priya, S.: Hydrogen-fuel-powered bell segments of biomimetic jellyfish. Smart Mater. Struct. **21**(4), 045013 (2012)
Tadesse, Y., Wu, L., Saharan, L. K.: Musculoskeletal system of bio-inspired robotic systems, Mechanical Engineering, vol. 138, no. 3 (2016)
Tomar, A., Tadesse, Y.: Multi-layer robot skin with embedded sensors and muscles, in SPIE Smart Structures and Materials + Nondestructive Evaluation and Health Monitoring. Int. Soc. Opt. Photonics. 979809–12 (2016)
Tomasi, C., Kanade, T.: Shape and motion from image streams under orthography: a factorization method. Int. J. Comput. Vision **9**(2), 137–154 (1992)
Villanueva, A., Smith, C., Priya, S.: A biomimetic robotic jellyfish (Robojelly) actuated by shape memory alloy composite actuators. Bioinspiration Biomim. **6**(3), 036004 (2011)
Wang, Z., Hang, G., Wang, Y., Li, J., Du, W.: Embedded SMA wire actuated biomimetic fin: a module for biomimetic underwater propulsion. Smart Mater. Struct. **17**(2), 025039 (2008)
Wilbur, C., Vorus, W., Cao, Y.: A lamprey-based undulatory vehicle. Neurotechnol. Biomim. Robots. p. 285 (2002)
Wu, L., de Andrade, M. J., Brahme, T., Tadesse, Y., Baughman, R. H.: A deformable robot with tensegrity structure using nylon artificial muscle. In: SPIE Smart Structures and Materials + Nondestructive Evaluation and Health Monitoring. pp. 97993 K-97993 K-12. International Society for Optics and Photonics (2016)
Wu, L., et al.: Nylon-muscle-actuated robotic finger. vol. 9431, pp. 94310I–94310I–12 (2015)
Wu, L. et al: Compact and low-cost humanoid hand powered by nylon artificial muscles. Bioinspiration Biomim. vol. 12 no. 2, (2017)
Yeom, S.-W., Oh, I.-K.: A biomimetic jellyfish robot based on ionic polymer metal composite actuators. Smart Mater. Struct. **18**(8), 085002 (2009)
Yip, M.C., Niemeyer, G.: High-performance robotic muscles from conductive nylon sewing thread. In: Robotics and Automation (ICRA), 2015 IEEE International Conference on. pp. 2313–2318. IEEE (2015)
Zhang, Z.: A flexible new technique for camera calibration. IEEE Trans. Pattern Anal. Mach. Intell. **22**(11), 1330–1334 (2000)

Yara Almubarak received her B.SC degree in Mechanical Engineering from The University of Texas at Dallas in 2016. She is currently working towards a MS. degree at the University of Texas at Dallas. Her research is focused on robotics, smart actuators, design, and manufacturing. She is one of the team member who received the 1st place in the 2016 Capstone Design Conference held in Columbus, Ohio, for a project entitled "Novel gastrointestinal injection array device".

Yonas Tadesse received his B.Sc degree from Addis Ababa University, M.Sc. degree from Indian Institute of Technology Bom-bay and Ph.D. from Virginia Polytechnic Institute and State University in 2000, 2005, and 2009, re-spectively, all in mechanical engineering. His research interests are in humanoid robotics, smart materials, mechatronic systems, multimodal energy harvesting, modeling, controls and biomimetics. He is currently an assistant professor of me-chanical engineering at the University of Texas at Dallas, and an affiliate faculty at the Alan MacDiarmid NanoTech Institute and electrical engnineering department at UTD. He has authored over 60 peer-reviewed publications. He is a member of ASME, SPIE, IEEE, NSBE, ASEE and ACS. His research on a hydrogen fuel-powered biomimetic jellyfish robot has attracted several media outlets from *BBC, Discov-ery News, Popular Mechanics, PC Maga-zine, New Scientist, LA Times, Wall Street Journal, Time Magazine, Dallas Morning News, Science Daily,* and *WIRED* magazine in 2012. He is a recipient of the 2015 ONR Young Investigator award.